Applied Engineering
2024; 8(2): 69-79
http://www.sciencepublishinggroup.com/j/ae
doi: 10.11648/j.ae.20240802.12
ISSN: 2994-7456 (Online)

Using Experiments, 3D Scanning, and CFD to Analyze the Variance in Energy Losses Through Pipe Elbows

Adam Pack[1], Steven Barfuss[2, *], Zachary Sharp[2]

[1]Hatch Associates Consultants, Minneapolis, United States
[2]Civil and Environmental Engineering Department, Utah State University, Logan, United States

Email address:

adam.pack@hatch.com (Adam Pack), steve.barfuss@usu.edu (Steven Barfuss), zac.sharp@usu.edu (Zachary Sharp)
*Corresponding author

To cite this article:

Adam Pack, Steven Barfuss, Zachary Sharp. (2024). Using Experiments, 3D Scanning, and CFD to Analyze the Variance in Energy Losses Through Pipe Elbows. *Applied Engineering, 8*(2), 69-79. https://doi.org/10.11648/j.ae.20240802.12

Received: 17 July 2024; **Accepted:** 20 August 2024; **Published:** 5 September 2024

Abstract: Pipe bends, or elbows, cause energy loss in pipelines due to the flow conditions they create. This energy loss has traditionally been approximated based on published minor loss coefficients, known as k-factors. However, the energy losses of elbows can vary based on geometric characteristics, which may not be accounted for in the published k-factors. The purpose of this research was to quantify the variance in energy loss resulting from elbows with geometric differences and to determine appropriate methods for approximating these variances using computational fluid dynamics (CFD). Eight polyvinyl chloride (PVC) elbows were physically tested in a hydraulic laboratory to determine the individual loss coefficients. The resulting data show that the minor loss coefficient k for two short-radius elbows of the same nominal size can vary by up to 51%. The same tests on two of the elbows were repeated using CFD, in which they were modeled two different ways: 1) using the ideal geometry and 2) using the actual geometry. The actual geometry was captured using 3D scanning. Each geometry was used in a series of simulations, and the results were compared to the experimental data. The CFD simulations were able to reproduce similar variances between the two elbows as displayed in the physical tests, although they were unable to reproduce the same k-factors. When compared to the experimental k-factor data, using the actual geometries captured by 3D scanning was not consistently more accurate than using idealized geometries.

Keywords: 3D Scanning of Pipes, CFD Simulation, Geometric Effects on Flow, Minor Loss Coefficient, Pipe Elbow Energy Loss

1. Introduction

Pipelines inevitably experience energy loss due to both friction losses and minor losses. Friction losses occur as flow interacts with the pipe wall. Minor losses occur when the flow path is changed, such as at pipe joints and bends. These losses require careful consideration when planning or analyzing a pipe system. Understanding cumulative energy loss helps maintain required flows or velocities, properly design pumps to recover lost energy, and optimize a piping system.

Friction losses depend on pipe roughness, flow velocity, and whether the flow is laminar or turbulent [1]. Minor losses vary with flow velocity as well, but are different for each type of fitting, bend, or valve that may exist in a pipeline. Minor losses can be quantified by multiplying a loss coefficient k, also referred to as the k-factor, by the velocity head (Equation 1).

$$h_L = k\frac{V^2}{2g} \tag{1}$$

Where h_L is the head loss (ft), V is the flow velocity (ft/s) and g is the gravitational acceleration (ft/s^2). The present work focuses on evaluating the minor losses through pipe elbows.

The k-factor provides a way to estimate the minor loss of an elbow. However, published k-factors rarely take proximity to other elbows, elbow type (other than bend angle), or flow velocity into account. Each of these factors affect the minor losses in elbows, as shown in laboratory research by Rahmeyer [2] and Coombs [3]. Variances in elbow geometry due to

manufacturing differences and variances in how the elbow is installed also affect the minor loss of the elbow [4].

Multiple methods have been used to better understand and quantify minor losses in elbows, including physical testing and numerical simulations.

1.1. Physical Testing

Physical tests of flow through elbows are the most commonly used and most accurate measure of head loss. Researchers have performed numerous tests to determine this head loss. Engineering publications often include generalized values for loss coefficients of pipe fittings, which are obtained from experimental data. In their text, Finnemore and Franzini list a separate value of k for short-, medium-, and long-radius elbows [5]. Potter and Wiggert present different values of k for different diameters and fitting types [6]. For a short-radius elbow, their published values of k range from 0.26 (for a large flanged elbow) to 1.5 (for a small threaded elbow).

Coffield et al. tested a 90-degree elbow and measured the pressure loss. Comparisons of the experimental k-factor and published k-factor correlations showed a maximum deviation of 30%. The authors note the large differences may be due to the limited data used for the published k-values [7].

William Rahmeyer performed hundreds of tests at the Utah Water Research Laboratory to explore the variation of head loss through pipe elbows. In 1999, he tested sixty 90-degree elbows, with 10 elbows each from 6 different manufacturers. Each elbow was a 2-inch malleable iron threaded elbow. The loss coefficient of the elbows varied by up to 22.6% between elbows of different manufacturers, and by up to 17.4% between elbows of the same manufacturer [2].

In 2003, Rahmeyer tested PVC pipe elbows that varied in size, mode of fabrication, and manufacturer. The loss coefficient varied by up to 30% between the same type of elbows provided by different manufacturers, and up to 62% for elbows of the same diameter and at the same velocity but different fabrication types. The fabrication types included injection molding, gluing, and thermowelding. The head loss also varied with changing flow velocities [8].

Yogajara et al. performed physical tests to calculate the loss coefficient of various pipe fittings, including one 1.5-inch pipe elbow. The average loss coefficient they calculated for the elbow was 0.85, which is approximately 5% less than the cited published value of 0.9 [9].

Research also shows the way elbows are connected to the upstream and downstream pipes affect the head loss. When joints vary from elbow to elbow, unknown head losses can be introduced or removed [4].

1.2. Numerical Modeling

Numerical modeling, specifically computational fluid dynamics (CFD), has become a viable way to analyze the flow disturbances caused by pipe elbows. A popular method to model pipe flow is by using a Reynolds-Averaged Navier-Stokes (RANS) turbulence model. RANS models approximate solutions to the Navier-Stokes equations by averaging the solution variables [10].

Well-calibrated RANS simulations can provide insights into the flow fields that are difficult to obtain during physical testing. Dutta et al. investigated the flow separation downstream of a pipe elbow while varying the Reynolds number [11]. Kim et al. performed similar simulations and found the results compared well with experimental data, particularly when the Reynolds number was between 50,000 and 200,000 [12].

Sami and Cui used a RANS model to validate the pressure loss due to a pipe elbow [13]. They approximated the geometry of a threaded elbow tested by Rahmeyer [14] and compared the calculated loss coefficient to the one obtained from physical testing. The RANS model produced a k-factor 18% less than the physical testing, which the researchers attribute to the inability to reproduce all the geometric irregularities of the physical elbow.

Coombs performed similar numerical tests using RANS models and compared the data to the values of k from physical tests of multiple pipe elbows. The tests included smooth, mitered, reducing, and expanding elbows. The values of k obtained from the CFD tests differed from the physical test data by $\pm$13.6% [3].

Gan and Riffat compared the k-factors of duct elbows produced by numerical simulations to experimental data. They note the significant differences in accuracy based on the turbulence model and differencing scheme used in the simulations [15].

Significant work has been done to quantify the benefits of using higher-fidelity models such as a large-eddy simulation (LES) as opposed to RANS models. LES models require more cells and computational power than RANS models, but can capture unsteady flow conditions more accurately. In one study, Röhrig et al. determined using LES to simulate flow through a pipe bend produced better representations of the turbulent flow than a RANS model and required approximately 550 times the number of cells the RANS model used. However, the authors state the RANS model adequately captured the total pressure loss across the pipe bend [16].

1.3. Applications of 3D Scanning

Some researchers have employed 3D scanning as a method to capture complex geometries more accurately. Because geometry affects flow characteristics, using geometry captured by 3D scanning can improve the accuracy of CFD models. This has been shown in open channel flow scenarios including flows in spillways, flumes, and rivers [17–19].

Various kinds of scanning have also been used to investigate pipe characteristics such as defects, corrosion, and roughness [20–22]. These scans are useful in inspecting pipe systems for signs of damage and age. Some researchers have also used 3D scans to produce geometries used in CFD simulations of pipe flow.

Sedlacek and Skovajsa used a 3D scanner to capture the geometry of an air intake system for a car engine. They used

the scanned geometry in a CFD simulation to find the best design for distributing air to the engine [23].

Christensen used 3D scanning to model an iron-based pipe with extensive deposition resulting in increased roughness and decreased diameter. He then performed numerical simulations using the 3D scanned geometry to calculate the friction factor of the pipe, which he compared to experimental data [24].

Čarija et al. used a 3D model of a Francis turbine partially produced by 3D scanning to validate CFD data to experimental data. Tests across the operating range of the turbine resulted in a maximum inaccuracy of $\pm 2\%$ for values of flow rate, torque, power, and efficiency. The numerical solution was performed using a RANS model [25].

1.4. Summary

Minor losses can be significant in piping systems and are often approximated using published minor loss coefficients. Experiments show the minor loss coefficients of pipe elbows vary based on physical properties such as pipe material and size, and flow properties such as fluid density and velocity.

CFD can produce accurate representations of physical systems, including pipe elbow flow. Simulation results show differences in minor loss coefficients for different elbows and flow rates, just as physical tests do.

3D scanning technology can digitize complex geometries, and scanned geometries have been used in various CFD applications to produce accurate representations of physical flow conditions. However, no known studies apply 3D scanning to analyzing minor losses in pipe fittings.

The objectives of the present work were to quantify the variance in loss coefficients for pipe elbows through physical laboratory tests as well as determining the impact of 3D scanning on simulating minor losses numerically.

To accomplish these objectives, eight 3-inch PVC elbows were tested in a laboratory to determine the minor loss coefficient at six flow rates. The set of elbows tested included six unique elbow types. The elbow types were differentiated based on radius of curvature and/or end connection type.

The physical test results from two of the elbows were compared to numerical models in which the elbow geometries were replicated using 3D scanning. Comparing a numerical simulation using the 3D scanned geometry to a simulation using an idealized geometry provided a quantitative difference in accuracy when compared to the physical data for the two geometry creation methods.

2. Materials and Methods

This section describes the procedure used for the physical testing of the pipe elbows, the creation of 3D models of two of the elbows, and the numerical simulations of the same two elbows.

2.1. Physical Testing

To obtain comparable minor loss coefficients, eight 3-inch diameter 90-degree elbows made of schedule 40 polyvinyl chloride (PVC) were tested. Table 1 shows details of the elbows tested. The abbreviations shown are used to refer to the elbows.

Table 1. *Inventory of elbows tested.*

Fitting Type	Radius	Abbreviation
Slip x Slip	Short	SxS 1
Slip x Slip	Short	SxS 2
Slip x Slip	Long	LR
Slip x Spigot	Short	SxSpig
Slip x Female Thread	Short	SxFPT
Slip x Male Thread	Short	SxMPT
Male Thread x Female Thread	Short	MPTxFPT 1
Male Thread x Female Thread	Short	MPTxFPT 2

The short radius elbows have a radius of curvature equal to the outside diameter of the pipe (1D), while the long radius elbow's radius of curvature is one and a half times the outside diameter (1.5D) [26]. All but the SxS 1, SxS 2, and LR elbows require additional fittings on one or both sides of the elbow to be installed in the pipeline. Figures 1-6 show top views of each type of elbow along with the required fittings. The SxS 2 and MPTxFPT 2 elbows are not shown but are visually identical to the SxS 1 and MPTxFPT 1 elbows.

Figure 1. *Slip x slip short radius elbow (SxS 1).*

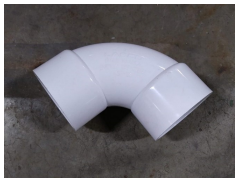

Figure 2. *Slip x slip long radius elbow (LR).*

Figure 3. *Slip x spigot short radius elbow (SxSpig).*

Figure 4. *Slip x female thread short radius elbow (SxFPT).*

Figure 5. *Slip x male thread short radius elbow (SxMPT).*

Figure 6. *Male thread x female thread short radius elbow (MPTxFPT 1).*

The fittings add significant length to the elbow and result in additional minor losses due to factors such as exposed threads and sudden changes in inner diameter. Because the fittings were required for some of these elbows to be connected to pipes, they were considered part of the associated elbows and the minor losses calculated are the aggregate minor losses from the elbows and any required fittings.

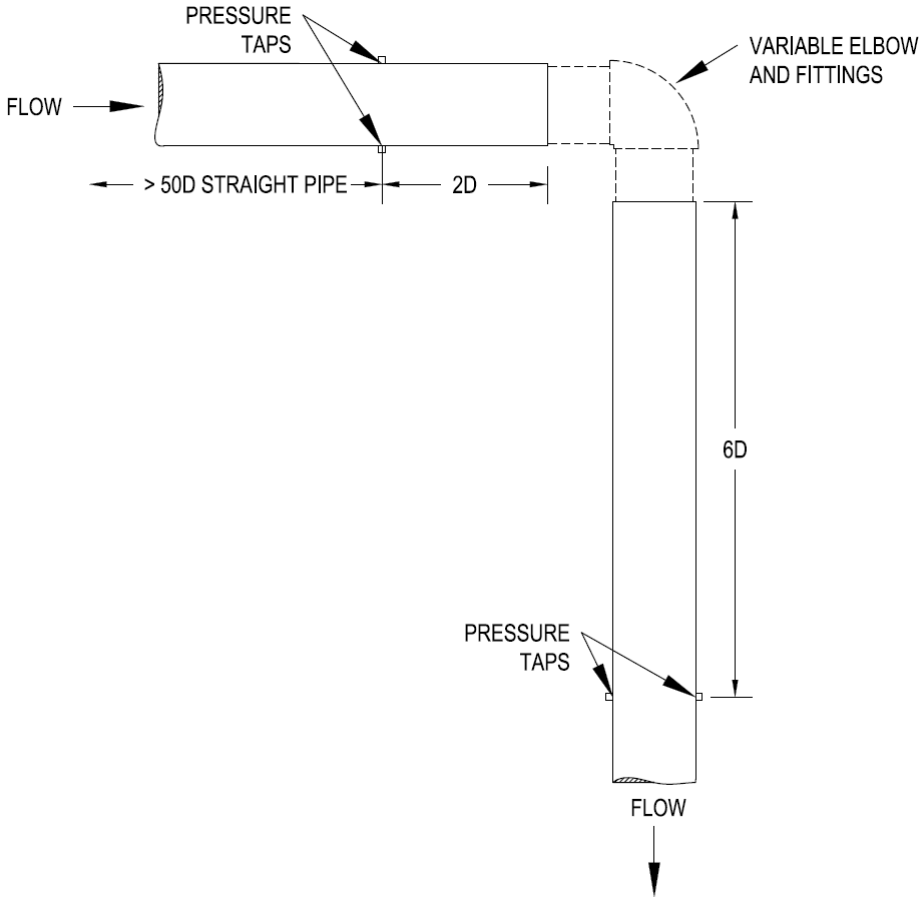

Figure 7. *Test setup for each physical test.*

PVC primer and cement were used to attach each elbow to an upstream and downstream length of PVC pipe. The initial direction of flow that was tested in the laboratory is referred to as direction A, and tests were repeated with flow going in the opposite direction (direction B). Figure 7 shows the test setup, which was identical for directions A and B other than the orientation of the elbow.

Pressure taps drilled on the spring-lines of the pipe (each side) provided access to measure the pressure upstream and downstream of each elbow. The pressure taps were located at two diameters (2D) upstream of the furthest upstream edge of the elbow or fitting, and at six diameters (6D) downstream of the downstream edge of the elbow or fitting. Tubes connected each pressure tap to a T-fitting, allowing for the upstream

pressure measurements to be combined and inserted as a single measurement into one side of a pressure transducer, with the downstream pressure measurements combined and inserted into the other side. The transducer measured the deflection of an inner diaphragm, which was converted to a pressure drop measurement.

Each elbow was installed and tested at flow rates of 50 gpm, 100 gpm, 150 gpm, 200 gpm, 250 gpm, and 300 gpm. Once the flow rate steadied during the test run, the flow rate measured by an electromagnetic flowmeter and the pressure loss measured by the pressure transducer were averaged for several minutes and recorded.

The outputs from the pressure transducer and flow meter were converted to a pressure loss in inches of water and a flow rate in cubic feet per second (cfs), respectively. To determine the net pressure loss between the two sets of taps, the friction factor f between the upstream and downstream pressure taps was calculated using the Swamee-Jain equation [27] and the friction loss was subtracted from the gross pressure loss obtained from the measured pressure differential.

Isolating the minor loss coefficient k in Bernoulli's equation [5] allowed for a direct solution of the net k-factor (Equation 2).

$$k = \frac{2g}{V^2}\Delta P - f\frac{L}{D} \tag{2}$$

Where g is the acceleration due to gravity (32.2 ft/s^2), V is the flow velocity (ft/s), ΔP is the pressure loss (ft), L is the length of pipe between pressure taps (ft), and D is the interior pipe diameter (ft).

After testing in direction A, new pressure taps (at 2D upstream and 6D downstream) drilled in the upstream and downstream pipes allowed for six of the elbows to be tested in direction B. The unused pressure taps were capped, and the same tests and calculations were carried out for the same flow rates as in direction A.

The SxS 2 and MPTxFPT 2 were only tested in direction A. It should be noted that there were no visual differences between these two elbows and the SxS 1 and MPTxFPT 1 elbows, respectively. The elbow geometries and test results of the SxS 2 and MPTxFPT 2 elbows were referenced for the geometry production and CFD modeling portions of the research.

2.2. Geometry Production

Prior to physical testing, calipers were used to capture the inner diameter of the upstream and downstream sides of the SxS 2 and MPTxFPT 2 elbows, along with the two fittings needed for the MPTxFPT 2 elbow. These physical measurements, along with drawings of the elbows from the manufacturer, were used to draft idealistic 3D models of the inner volumes of each elbow.

These models were approximate, as precise diameters were not known along the entire interior length of each elbow. The CAD models did not consider any geometric irregularities due to PVC cement or gaps between fittings and pipes. Figure 8 shows the 3D CAD model of the MPTxFPT 2 elbow and associated fittings.

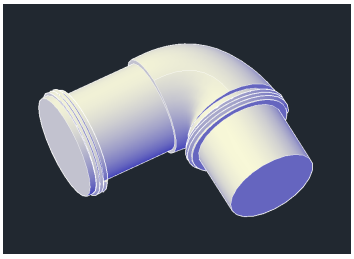

Figure 8. *CAD model of MPTxFPT 2 elbow.*

To capture a 3D scan of the inside of each elbow, the SxS 2 and MPTxFPT 2 elbows were cut off from the upstream and downstream pipes. Each elbow was then filled with Perfect Cast, a plaster-like casting material, according to the manufacturer's instructions. The pipe elbow was then removed from the cast. Measurements of the diameter on each end of the MPTxFPT 2 elbow showed the cast was an average of 0.07% smaller than the elbow due to shrinkage while curing.

Inspecting each cast allowed for comparison to the inner geometry of the SxS 2 and MPTxFPT 2 elbows to the inner geometry of the SxS 1 and MPTxFPT 1 elbows. While the elbows and fittings themselves were theoretically identical between the two sets of tests, a few differences exist between the geometries because of installation. The same procedure was used to install all elbows, but the following differences were observed:

1. The threaded fittings were tightened more on the MPTxFPT 2 elbow, so less threads were exposed than in the MPTxFPT 1 elbow.
2. The MPTxFPT 2 elbow had a larger gap between the pipe and fitting on the upstream side than the MPTxFPT 1 elbow
3. The MPTxFPT 2 elbow had a smaller gap between the pipe and fitting on the downstream side than the MPTxFPT 1 elbow
4. The SxS 2 elbow had an 0.34-inch gap between the pipe and the fittings on the downstream side, while the SxS 1 elbow had virtually no gap on that side.

Each cast was scanned using an EinScan-SP 3D scanner. The EinScan-SP scanner uses structured-light technology to capture geometries and has a published accuracy of 0.05 mm [28]. Several scans of each cast allowed the scanner to capture the entire surface.

Figure 9 shows the scanned surface of the cast of the MPTxFPT 2 elbow. Measurements of the MPTxFPT 2 scanned geometry showed the average inner diameter on either end of the elbow was 0.22% less than the diameter of the physical elbow. No attempt was made to scale the scanned models to better match the physical measurements because the diameter differences could vary at each point of the elbow.

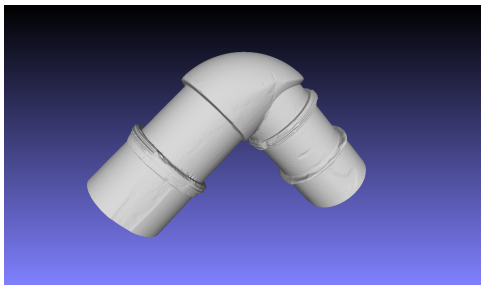

Figure 9. *3D scanned model of MPTxFPT 2 elbow.*

2.3. CFD Modeling

The authors used STAR-CCM+, a commercially available software, to numerically model the SxS 2 and MPTxFPT 2 elbows so the numerical losses could be compared to the physical test data.

STAR-CCM+ includes capabilities to perform steady and unsteady flow simulations. Unsteady simulations can better represent turbulent flows but are more computationally expensive. Because the goal of the research was to determine the effects of geometry on simulation accuracy rather than produce the most accurate simulation, a steady simulation was used to save on computational time.

The steady models in STAR-CCM+ are RANS models that approximate solutions to the Navier-Stokes equations. The Realizable K-Epsilon Two-Layer model was chosen for its ability to accurately model the boundary layers near the pipe wall [10]. The flow was modeled as fully turbulent and three-dimensional, with water at a constant density. The density and kinematic viscosity were inputs based on the temperature of the water during physical testing.

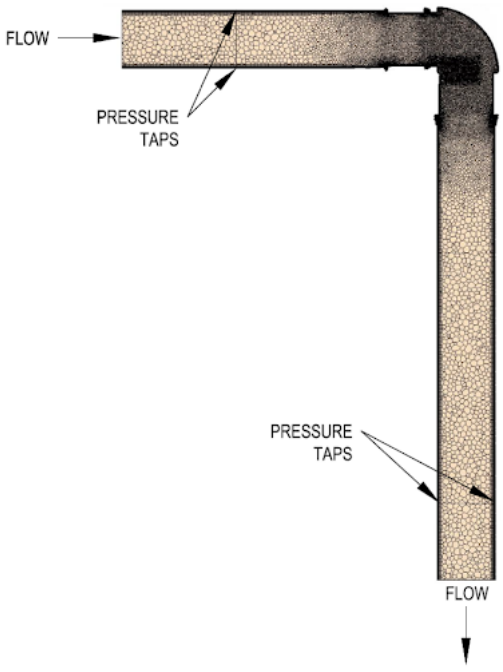

Figure 10. *Horizontal cross-section of volume mesh for 3D scanned MPTxFPT 2 geometry.*

The simulations in this research used polyhedral meshes, which create cells with many faces and neighboring cells. The simulations also employed the prism layer mesher and the surface remesher. The prism layer mesher allows for finer cells to be generated near the pipe walls, thus accurately capturing the boundary layer conditions. The surface remesher improves the overall quality of the surface mesh [10]. Figure 10 shows a cross section of the volume mesh used for the MPTxFPT 2 elbow simulation.

As seen in Figure 10, certain areas of the mesh were refined to better capture complex flow fields using volumetric controls in those areas. Less critical areas of the simulation were left with a relatively coarse mesh, thus limiting the number of cells needed and computational cost. For all elbows, the inside corner of the elbow and surrounding volume were refined to more accurately simulate flow separation. Any areas of the meshed volume including threads or small gaps were also refined to capture the finer details in those areas. The SxS 2 drawn geometry had no gaps or threads, but the three other elbows included these additional refinements along with the inside corner refinement.

It was also important to refine the overall mesh base size until the solution converged. This ensured the solution was not dependent on the level of mesh refinement. A mesh refinement procedure developed by Celik et al. was carried out for all four elbow geometries [29]. Each mesh was refined by decreasing the base mesh size. Then, the simulation was run and the k-factor for each resulting mesh at the flow rates of 50 gpm and 300 gpm was calculated. The author assumed that if the mesh was sufficiently refined at the minimum and maximum flow rates, the mesh would be sufficiently refined at the intermediate flow rates. Three base sizes, 0.43 inches, 0.30 inches, and 0.22 inches, were used to generate meshes and calculate k-factors.

Celik et al. states the mesh refinement procedure does not perform well for situations with very small changes in the critical variable with mesh refinement [29]. In this case, the k-factor was the critical variable, and because the k-factors were small numbers with even smaller changes from simulation to simulation, the mesh refinement method did not produce meaningful results.

Because this refinement method did not apply to the situation, the percent difference in k-factor from one refinement level to the next was used as the convergence criteria. The difference in k-factors from the second-finest (0.30 in. base size) to the finest (0.22 in. base size) mesh was less than 1.0% for each elbow geometry and flow rate. This level of convergence was determined satisfactory, and the finest mesh base size (0.22 inches) was used for all numerical simulations. Table 2 shows the final mesh parameters used for each simulation.

Table 2. *Mesh parameters used for all simulations.*

Parameter	Value
Base Size	0.22 in.
Target Surface Size	Varied
Minimum Surface Size	0.022 in.
Surface Growth Rate	Slow
Number of Prism Layers	15
Prism Layer Stretching	1.3
Prism Layer Total Thickness	0.22 in.
Volume Growth Rate	1.05
Maximum Tet Size	0.32 in.
Mesh Optimization Cycles	3
Mesh Quality Threshold	0.8

The physical tests included more than fifty diameters (50D) of upstream straight pipe length, which is enough to theoretically create a fully developed velocity profile upstream of the elbow [30]. To replicate these physical conditions, a fully developed velocity profile was uploaded as the inlet condition in each numerical simulation. Pressure probes were placed in the simulation at the farthest outside edges of the mesh at the same locations as the physical upstream and downstream taps.

Each simulation was run until the solution converged. Convergence was determined by monitoring the residuals and the pressure drop across the elbow, which was the variable of interest, at each iteration. Once the residuals and pressure drop stabilized, the pressure drop and flow rate were recorded.

Using the simulated flow rate and the difference between the upstream and downstream pressures, the value of k was calculated in the same manner as for the physical tests. The simulated k-factor was compared to the physical k-factor.

Figure 11 shows a diagram of the overall testing methodology.

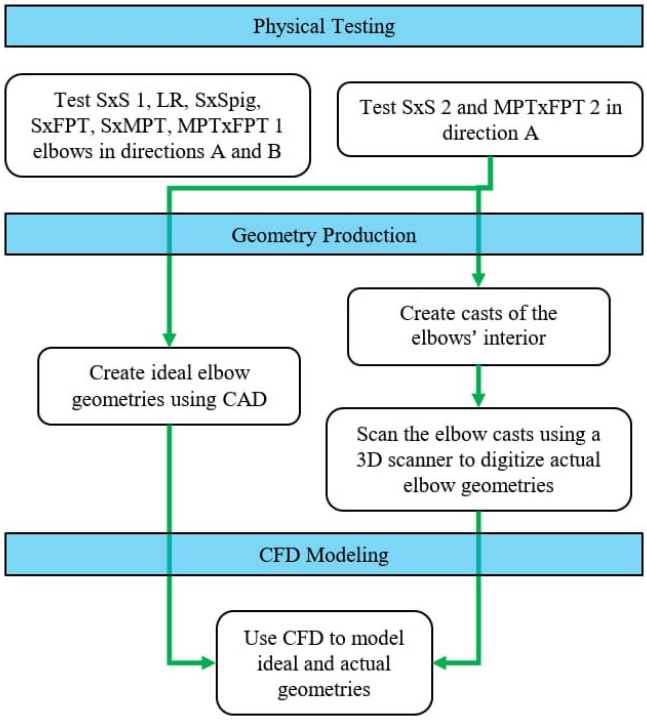

Figure 11. *Workflow diagram.*

3. Results

This section presents and compares the data from both the physical tests and CFD simulations. Eight elbows were tested in the laboratory, with two of the elbows also modeled and simulated numerically.

3.1. Physical Data

Tests of six elbows in two directions provided data for comparing the pressure loss due to each elbow. Figure 12 shows the calculated values of k for the elbows in directions A and B for direct comparison.

The results of the tests in each direction follow similar trends, but the pressure loss for each elbow differs in each direction. Table 3 shows the percent difference of the average values of k in directions A and B.

The LR and SxFPT elbows showed the greatest percent deviation in k between directions. The LR elbow is manufactured to be symmetrical, so the relatively large percent difference is likely primarily due to the small value of k when

compared to the other elbows. The smaller value of k results in larger percent changes with relatively slight changes in k.

For the short radius elbows, the largest difference in average k-factors existed between the SxS 1 and MPTxFPT 1 elbows. Considering both flow directions, the average k-factor varied by up to 50.2% between these elbows. These results corroborate Rahmeyer's conclusion regarding the large variance in energy losses for pipe elbows, even when those elbows have the same nominal diameter and radius of curvature.

The SxS 2 and MPTxFPT 2 elbows were placed in direction A and tested. The average k-factor between the SxS 1 and SxS 2 elbows was 7.5% different, and the average k-factor between the MPTxFPT 1 and MPTxFPT 2 elbows was 12.4% different. The difference in k-factors is likely due to variations in the elbow and fitting geometries, which were observed when producing the scanned geometries. A combination of these factors and unobservable surface differences likely led to the difference in experimental k-factors for each elbow.

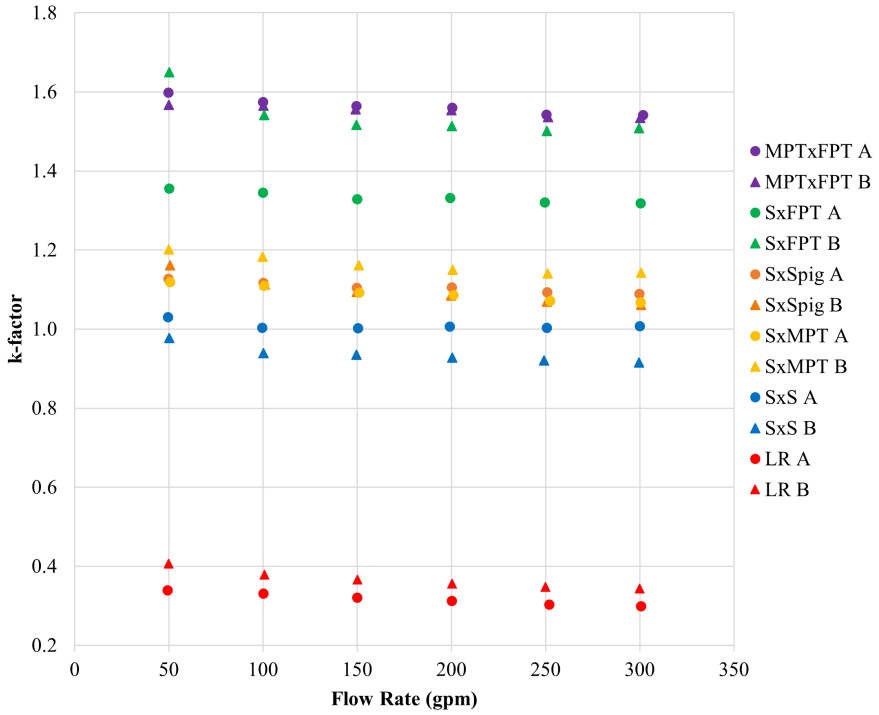

Figure 12. *Flow velocity and k-factor of elbows in directions A and B from physical tests.*

Table 3. *Difference in k-factors in directions A and B.*

Elbow	Average k-factor Direction A	Average k-factor Direction B	Percent Difference
SxS 1	1.01	0.94	-7.6%
SxSpig	1.24	1.10	-12.4%
LR	0.45	0.37	-21.3%
SxMPT	1.23	1.16	-5.4%
SxFPT	1.48	1.54	4.1%
MPTxFPT 1	1.56	1.55	-0.7%

3.2. CFD Simulation Data

The physical tests of the SxS 2 and MPTxFPT 2 elbows were repeated numerically using CFD. The CFD simulations underpredicted the k-factor from the physical tests in all cases, which is similar to the results produced by Sami [13]. The percent difference of the k- factors produced by the simulations compared to the physical data fall within the range of percent differences produced by Coombs [3].

Figure 13 shows the k-factor at each flow rate for the physical and numerical tests, and Table 4 shows the average simulated k-factor and percent difference from the k-factor measured in the physical tests.

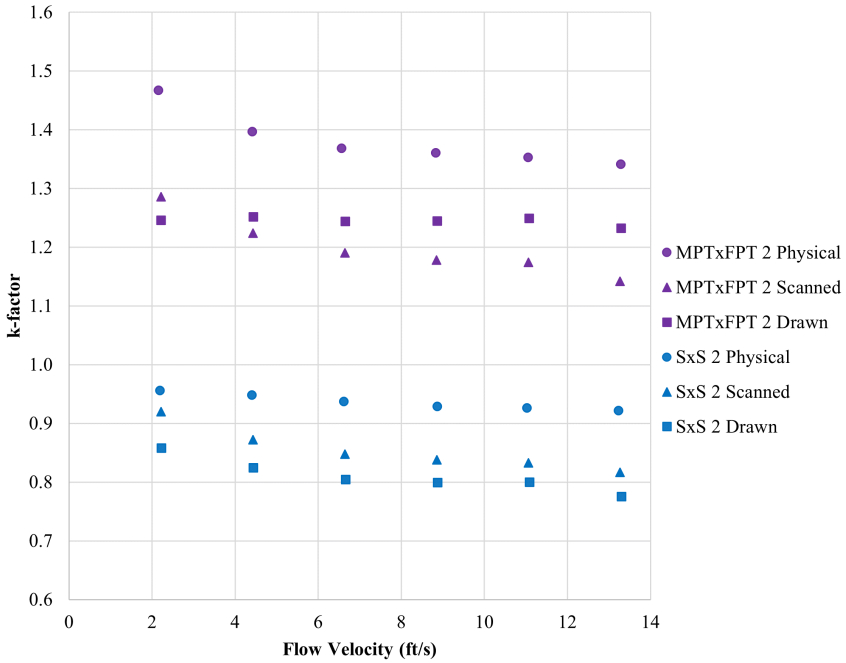

Figure 13. *Flow velocity and k-factor from physical and numerical tests, all in direction A.*

Table 4. *Average k-factor and percent difference for each numerical simulation.*

Elbow	Geometry	Average k-factor		% difference in average k-factor
		Simulated	Physical	
SxS 2	Drawn	0.81	0.94	-13.5%
	Scanned	0.85		-8.8%
MPTxFPT 2	Drawn	1.24	1.38	-9.9%
	Scanned	1.20		-13.2%

4. Discussion

The physical test results highlight the importance of using the correct k-factor in systems where minor losses are significant. For example, if the true elbow k-factor is 50% higher than the k-factor used in calculations during the design of a plumbing system, the energy loss resulting from the elbows would be 50% higher than predicted. If a pump is used to supply water and a certain flow rate is needed, this would potentially result in much higher pumping costs than expected.

The CFD simulations showed that the different procedures for creating elbow geometries resulted in different k-factors. The scanned geometry of the SxS 2 elbow resulted in an average k-factor 4.7% closer to the k-factor from the physical tests than the drawn geometry. However, in the case of the MPTxFPT 2 elbow, the drawn geometry produced a k-factor 3.3% closer to the physical data than the scanned geometry.

This shows that neither geometry preparation method better replicated the physical data in all cases. However, both geometry production methods produced CFD results showing similar relative differences between the SxS 2 and MPTxFPT 2 k-factors as in the physical tests. This shows that the CFD results may be more useful for comparing relative differences in k-factor rather than determining precise values of the k-factor.

The scanned geometry included details of the elbow as it was installed, including details not included in the drawn geometry. One would assume the inclusion of these details would make the simulation produce a k-factor closer to that from the physical tests, but for the MPTxFPT 2 elbow the drawn geometry showed a higher k-factor and pressure loss, bringing it closer to the physical data, than the scanned geometry.

The drawn geometries generally have sharper edges than the scanned geometries, which, while less accurate geometrically, may have increased the pressure loss and consequently resulted in a k-factor closer to that produced by the physical data. Costa illustrated the influence of sharp edges on minor-loss coefficients in T-junctions. They found that a T-junction with sharp edges had a k-factor up to 20% higher than a T-junction with smoother edges [31]. Assuming the sharpness of edges affects elbow k-factors in a similar way and have more effect than the details added by 3D scanning, this could explain why the drawn MPTxFPT 2 geometry had a higher k-factor

than the scanned geometry.

5. Conclusions

This study aimed to quantify the variance in energy losses through pipe elbows with different geometric characteristics and to evaluate the effectiveness of using 3D scanning and CFD simulations to approximate these variances. The novelty of this research lies in its comparison of physical testing and numerical modeling using both idealized geometries and actual geometries captured by 3D scanning.

To measure energy loss through each elbow, physical laboratory tests were conducted on eight 3-inch PVC elbows. The minor loss coefficients of each elbow was calculated at various flow rates. Two elbows were modeled in 3D, once using idealized dimensions and once using 3D scans of the actual elbow geometries. These models were then used in CFD simulations to compare the numerical results with the experimental data.

The primary results of the study are:

1. The minor loss coefficients for short-radius elbows of the same nominal size can vary by up to 51%.
2. Physical tests showed significant differences in minor loss coefficients based on elbow type, manufacturer, and installation conditions.
3. CFD simulations using idealized geometries underpredicted the k-factors compared to physical tests.
4. 3D scanned geometries did not consistently produce more accurate k-factors than idealized geometries.
5. Both geometry production methods showed similar relative differences in k-factors for the CFD simulation results as observed in physical tests.

The limitations of the present work and opportunities for future research include:

1. This study was limited to 3-inch PVC elbows; future research should explore a wider range of pipe sizes, materials, and flow conditions.
2. Further investigation is needed to determine the conditions under which 3D scanned geometries provide more accurate results than idealized geometries.
3. Future studies should consider the impact of different turbulence models on the accuracy of CFD simulations for minor loss measurement.

Abbreviations

CFD	Computational Fluid Dynamics
PVC	Polyvinyl Chloride
RANS	Reynolds-Averaged Navier-Stokes

ORCID

0000-0002-4717-0053 (Adam Pack)
0000-0002-6954-0836 (Steven Barfuss)
0000-0002-6680-6870 (Zachary Sharp)

Author Contributions

Adam Pack: Conceptualization, Data curation, Formal Analysis, Investigation, Methodology, Project administration, Software, Visualization, Writing - original draft, Writing - review & editing

Steven Barfuss: Conceptualization, Funding acquisition, Methodology, Project administration, Resources, Supervision, Validation, Writing - review & editing

Zachary Sharp: Methodology, Software, Validation, Writing - review & editing

Funding

Utah State University financially supported this work completed as part of Adam Pack's master's thesis research.

Conflicts of Interest

The authors declare no conflicts of interest.

References

[1] I. Goswami, Civil Engineering All-In-One PE Exam Guide: Breadth and Depth. McGraw-Hill Education, 2015.

[2] W. J. Rahmeyer, "Pressure loss coefficients of threaded and forged weld pipe fittings for ells, reducing ells, and pipe reducers," ASHRAE Transactions, vol. 105, p. 334, 1999.

[3] H. J. Coombs, "Pressure loss coefficients for large mitered elbows with diameters ranging from 36-inches to 144-inches," Master's thesis, Utah State University, Logan, UT, 2019. https://doi.org/10.26076/zvsk-fm62

[4] P. Wichowski, T. Siwiec, and M. Kalenik, "Effect of the concentration of sand in a mixture of water and sand flowing through pp and pvc elbows on the minor head loss coefficient," Water, vol. 11, no. 4, p. 828, 2019. https://doi.org/10.3390/w11040828

[5] E. J. Finnemore, J. B. Franzini, et al., Fluid mechanics with engineering applications, vol. 10. McGraw-Hill New York, 2002.

[6] M. C. Potter and D. C. Wiggert, Schaum's outline of fluid mechanics. McGraw-Hill Education, 2021.

[7] R. Coffield, P. Brooks, and R. Hammond, "Piping elbow irrecoverable pressure loss coefficients for moderately high reynolds numbers," Tech. Rep. WAPD-T-3064, Bettis Atomic Power Lab., West Mifflin, PA, 1995.

[8] W. J. Rahmeyer, "Pressure loss data for PVC pipe elbows, reducers, and expansions," ASHRAE Transactions, vol. 109, p. 230, 2003.

[9] L. Yogaraja, N. Liyanagamage, and K. De Silva, "Comparison of experimental results with empirical relationships for energy losses in pipe flow," in 2021 Moratuwa Engineering Research Conference (MERCon), pp. 522-527, IEEE, 2021. https://doi.org/10.1109/MERCon52712.2021.9525661

[10] Siemens, "Simcenter STAR-CCM+ user guide version 2020.3," Siemens Digital Industries Software, 2020.

[11] P. Dutta, S. K. Saha, N. Nandi, and N. Pal, "Numerical study on flow separation in 90° pipe bend under high reynolds number by k-ε modelling," Engineering Science and Technology, an International Journal, vol. 19, no. 2, pp. 904-910, 2016. https://doi.org/10.1016/j.jestch.2015.12.005

[12] J. Kim, M. Yadav, and S. Kim, "Characteristics of secondary flow induced by 90-degree elbow in turbulent pipe flow," Engineering Applications of Computational Fluid Mechanics, vol. 8, no. 2, pp. 229-239, 2014. https://doi.org/10.1080/19942060.2014.11015509

[13] S. Sami and J. Cui, "Numerical study of pressure losses in close-coupled fittings," HVAC & R Research, vol. 10, no. 4, pp. 539-552, 2004. https://doi.org/10.1080/10789669.2004.10391119

[14] W. J. Rahmeyer, "Pressure loss coefficients for close-coupled pipe ells," ASHRAE Transactions, vol. 108, p. 390, 2002.

[15] G. Gan and S. Riffat, "k-factors for HVAC ducts: Numerical and experimental determination," Building Services Engineering Research and Technology, vol. 16, no. 3, pp. 133-139, 1995. https://doi.org/10.1177/014362449501600303

[16] R. Röhrig, S. Jakirlić, and C. Tropea, "Comparative computational study of turbulent flow in a 90pipe elbow," International Journal of Heat and Fluid Flow, vol. 55, pp. 120-131, 2015. https://doi.org/10.1016/j.ijheatfluidflow.2015.07.011

[17] A. G. Andersson, P. Andreasson, and T. Staffan Lundström, "CFD-modelling and validation of free surface flow during spilling of reservoir indown-scale model," Engineering Applications of Computational Fluid Mechanics, vol. 7, no. 1, pp. 159-167, 2013. https://doi.org/10.1080/19942060.2013.11015461

[18] T. J. Ashby, "Evaluating the hydraulic performance of digital photogrammetry-derived 3-dimensional models of a hydraulic structure using computational fluid dynamics," Master's thesis, Utah State University, Logan, UT, 2020. https://doi.org/10.26076/d1a7-8c5a

[19] G. Mandlburger and C. Briese, "Using airborne laser scanning for improved hydraulic models," in International Congress on Modelling and Simulation, pp. 731-738, 2007.

[20] J.-H. Lee and S.-J. Lee, "Application of laser-generated guided wave for evaluation of corrosion in carbon steel pipe," Ndt & E International, vol. 42, no. 3, pp. 222-227, 2009. https://doi.org/10.1016/j.ndteint.2008.09.011

[21] M. Lepot, N. Stanić, and F. H. Clemens, "A technology for sewer pipe inspection (part 2): Experimental assessment of a new laser profiler for sewer defect detection and quantification," Automation in Construction, vol. 73, pp. 1-11, 2017. https://doi.org/10.1016/j.autcon.2016.10.010

[22] N. Stanić, F. H. Clemens, and J. G. Langeveld, "Estimation of hydraulic roughness of concrete sewer pipes by laser scanning," Journal of Hydraulic Engineering, vol. 143, no. 2, p. 04016079, 2017. https://doi.org/10.1061/(ASCE)HY.1943-7900.0001223

[23] F. Sedlacek and M. Skovajsa, "Optimization of an intake system using CFD numerical simulation," Proceedings in Manufacturing Systems, vol. 11, no. 2, p. 71, 2016.

[24] R. T. Christensen, "Age effects on iron-based pipes in water distribution systems," Master's thesis, Utah State University, Logan, UT, 2009. https://doi.org/10.26076/28aa-15e2

[25] Z. Čarija, Z. Mrša, and S. Fućak, "Validation of francis water turbine CFD simulations," Strojarstvo: časopis za teoriju i praksu u strojarstvu, vol. 50, no. 1, pp. 5-14, 2008.

[26] Spears, "Schedule 40 white." Available from: https://www.parts.spearsmfg.com/ProductDetails.aspx (accessed 30 April 2021).

[27] P. K. Swamee and A. K. Jain, "Explicit equations for pipe-flow problems," Journal of the hydraulics division, vol. 102, no. 5, pp. 657-664, 1976. https://doi.org/10.1061/JYCEAJ.0004542

[28] SHINING 3D, "EinScan-SP specs desktop 3D scanner," 2020. Available from: https://www.einscan.com/einscan-sp (accessed 20 May 2021).

[29] I. B. Celik, U. Ghia, P. J. Roache, and C. J. Freitas, "Procedure for estimation and reporting of uncertainty due to discretization in CFD applications," Journal of fluids Engineering-Transactions of the ASME, vol. 130, no. 7, 2008. https://doi.org/10.1115/1.2960953

[30] L. H. Hellström, M. B. Zlatinov, G. Cao, and A. J. Smits, "Turbulent pipe flow downstream of a bend," Journal of Fluid Mechanics, vol. 735, 2013. https://doi.org/10.1017/jfm.2013.534

[31] N. Costa, R. Maia, M. Proenca, and F. Pinho, "Edgeeffects on the flow characteristics in a 90 deg tee junction," J. Fluids Eng., vol. 128, no. 6, pp. 1204-1217, 2026, https://doi.org/10.1115/1.2354524